ON THE USE OF CONTINUOUS-WAVELET TRANSFORM FOR FAULT LOCATION IN DISTRIBUTION POWER NETWORKS

A. Borghetti[1], S. Corsi[2], C.A. Nucci[1], M. Paolone[1], L. Peretto[1], R. Tinarelli[1]
[1] Dept. of Electrical Engineering, University of Bologna, Bologna, Italy
[2] CESI, Milan, Italy

Abstract – The paper illustrates a procedure, based on the continuous-wavelet transform, for the analysis of voltage transients due to line faults and discusses its application to fault location in power distribution networks. The analysis carried out allows us to infer that correlation does exist between some characteristic frequencies of the transformed signal and specific paths in the network covered by the traveling waves originated by the fault. This correlation provides useful information for the location of the faulted section in a MV distribution network starting from the recorded voltage transients at one or more busses. The presented approach can find a useful application in the realization of a distributed measurement and fault locating system. A brief description of the basic concepts of such a system and a first estimation of the relevant uncertainty are also provided in the paper.

Keywords: Fault location, power distribution networks, continuous wavelet transform.

1 INTRODUCTION

Fault location in MV distribution network is a research topic that is receiving increased attention in recent years, due both to increased power quality requirements and to the availability of improved measurement and monitoring systems. In addition, the increased installation of distributed generation resources in the network requires the overhaul of traditional procedures based on automatic switching systems.

The most promising approach appears to be the application of appropriate signal processing techniques to the voltage/current transients produced by short circuit events and recorded at one or more locations in the distribution network.

Recent contributions to the subject are based on the use of wavelet transforms (e.g. [1-4]), usually adopting the discrete-wavelet transform (DWT), due to its straightforward implementation and the reduced computational time it requires.

In this paper, use is made of the continuous-wavelet transform (CWT) algorithm. Compared to the DWT algorithm, the CWT one allows performing a more detailed analysis of the spectrum energy of the fault transient. Such a feature is used to detect the distinctive frequencies of propagation and reflections of the voltage transients generated by the fault in the distribution network. This information, associated with the knowledge of the network topology and the wave propagation velocity along the lines, can be used for inferring the location of the fault.

The paper is structured as follows.

Section 2 describes the computational procedure for the general case of nonsymmetrical faults with non zero impedance. That section presents also a sensitivity analysis of the results, carried out by means of simulations on a distribution network for different conditions (e.g. neutral grounding characteristics), with various types of fault and, obviously, for various fault locations. The presence of distributed generators is also taken into account. The models adopted for the electromagnetic transient simulations are briefly discussed in the Appendix, which reports also the system data.

The described CWT based algorithm is conceived to be combined with a measurement system aimed at acquiring both the starting time of the transient and the relevant waveform. Section 3 describes a possible architecture of such a measurement system for the acquisition of voltage transients. In order to build a distributed fault location system, each terminal is equipped with a GPS synchronization device able to detect the initial time of the transient.

The concluding section summarizes the main contributions of the paper and the aspects requiring additional research efforts.

2 FAULT LOCATION INFORMATION PROVIDED BY CONTINUOUS WAVELET TRANSFORM

The continuous wavelet transform (CWT) of a signal $s(t)$ is the integral of $s(t)$ multiplied by time translation and scale dilatation versions of a function with finite energy $\psi(t)$, called mother wavelet. This process produces wavelet coefficients $C(a,b)$, which can be seen as "resemblance indexes" between the signal and the wavelet located at position b (time shifting factor) and of positive scale a:

$$C(a,b) = \int_{-\infty}^{\infty} s(t) \frac{1}{\sqrt{a}} \psi^*\left(\frac{t-b}{a}\right) dt \qquad (1)$$

where * denotes complex conjugation.

One can also write (e.g. [5])

$$F(C(a,b)) = \sqrt{a}\, \Psi^*(a\omega)\, S(\omega) \qquad (2)$$

where $F(C(a,b))$, $S(\omega)$ and $\Psi(\omega)$ are the Fourier transforms of $C(a,b)$, $s(t)$ and $\psi(t)$ respectively.

Equation (2b) shows that if the mother wavelet is a bandpass filter function in the frequency-domain, by using CWT the frequency-domain local feature of the signal can be extracted. According to the Fourier transform theory, if the center frequency of the mother wavelet $\Psi(\omega)$ is F_0, then that of $\Psi(a\omega)$ is F_0/a. Therefore, in the analyzed result, different scales extract different frequencies from the original signal, and, in particular, larger scales correspond to lower frequencies. Moreover, the quality factor (equal to center fre-

quency/bandwidth) of the analyzing wavelet $\Psi(a\omega)$ is constant. While in windowed-Fourier analysis the frequency resolution is constant and depends on the width of the chosen window, in the wavelet approach the width of the window varies as a function of a, thus allowing a kind of time-windowed analysis, different at the various scales a.

Various types of mother wavelets have been proposed in the literature. Provided that the mother wavelet satisfies some specific conditions, the signal can also be reconstructed from the transform coefficients, In this paper, the so-called Morlet wavelet is chosen as mother wavelet $\psi(t)$

$$\psi(t) = e^{-t^2/2} e^{i2\pi F_0 t} \tag{3}$$

Unlike the discrete wavelet transform, CWT can operate at any scale, from that of the original signal up to some maximum scale. CWT is also continuous in terms of shifting: during computation, the analyzing wavelet is shifted smoothly over the full domain of the analyzed function.

We perform CWT analysis on the voltage transient recorded after the fault in a bus of the distribution network. The transient recording has the limited duration (few milliseconds) allowed by the intervention time of the protections.

The method that we propose is described in what follows. As scales a are related to frequency values, the summation of the squared values of all coefficients corresponding to the same scale (which we shall call CWT signal energy) identifies the weight of such a frequency component of signal $s(t)$. By inspecting the relative maximum peaks of the graph of the summation results, the most significant frequency component of the signal are then detected. In the following we shall call these values as CWT-identified frequencies of the transient. These frequency values are caused by propagation phenomena along the lines of the fault-originated traveling waves and their reflections at discontinuity points. Therefore, each fault location can be associated to some theoretical frequency values calculated as a function of the length of the path covered by the traveling waves, of the propagation velocities along the lines and of the types of reflections. The match between these frequency values and those identified by the CWT procedure can provide useful information for the fault location.

By using the simulation results obtained from an electromagnetic transient program (specifically, EMTP-RV v.1.1) and assuming the distribution network configuration shown in Figure 1 (whose details are given in the Appendix), in the following paragraph we apply the method for the simple case of a balanced (three-phase) fault. The procedure is then extended and applied to the case of nonsymmetrical faults.

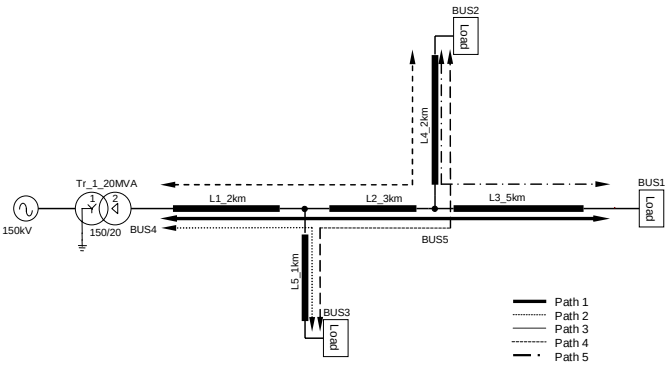

Figure 1 Power distribution network configuration and paths covered by traveling waves casused by a fault at bus 1.

2.1 Balanced faults

Figure 2 shows the simulated voltage transients at three different observation points of the network due to a zero-impedance three-phase fault at bus1, i.e. the terminal end of the main feeder.

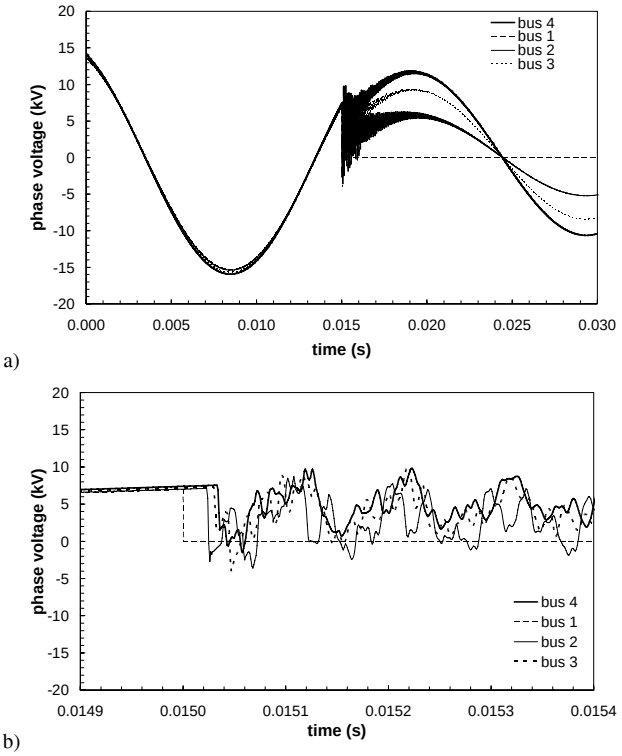

Figure 2 Voltage transients on a phase due a three-phase fault at bus 1 as observed at three different nodes (bus 2, bus 3 and bus 4), of the power distribution network shown in Figure 1: a) general behavior, b) detailed view.

Figure 1 also illustrates six paths covered by traveling waves originated by a fault at bus 1. The traveling waves are reflected at the line terminations and at the fault location. Paths with partial reflections at the point where more lines converged are here disregarded. Only three paths (namely paths 1, 2 and 3) reach the observation point, assumed at bus 4, i.e. the sending end of the main feeder. Path 1 is associated to a period given by a traveling time equal to 4 times L1+L2+L3 divided by the speed of propagation, as the traveling wave experience reflections of opposite sign at the fault location

(bus 1) and at the sending end of the main feeder (bus 4). For paths 2 and 3, the associated periods are given by the traveling time relevant to the double path lengths (L1+L2+L4 and L1+L5, respectively), as the traveling wave is reflected at the line terminations.

Figure 3 presents the results of the CWT analysis of the voltage transient of Figure 2 at the observation point (bus 4). Table 1 compares the results inferred theoretically by assuming, in a first approximation, the traveling wave velocity equal to the speed of light with those identified from the peaks in Figure 3.

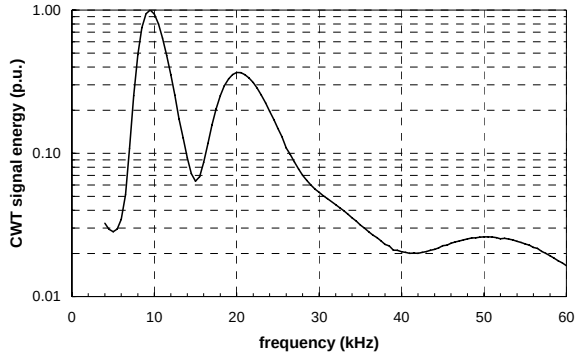

Figure 3 Results of the CWT analysis of the voltage transient of Figure 2 at bus 4. The values are in per unit with respect to the maximum ($1.25 \cdot 10^{12}$ V^2s).

Table 1 Frequency values theoretically associated to the paths covered by the traveling waves originated by a balanced fault at bus 1, and values identified by the CWT analysis.

Path	length	theoretical frequency value (traveling wave at light speed) (kHz)	CWT identified frequency value (kHz)
L1+L2+L3	4x10km	7.5	9.5
L1+L2+L4	2x7km	21.4	20.5
L1+L5	2x3km	50	50.5

Figure 4 and Table 2 show the results for the case of a balanced fault at bus 5. In this case only two paths are of interest: L1+L2, with opposite sign reflections at the fault location and at the main feeder sending end and L1+L5, with reflection at the line terminations.

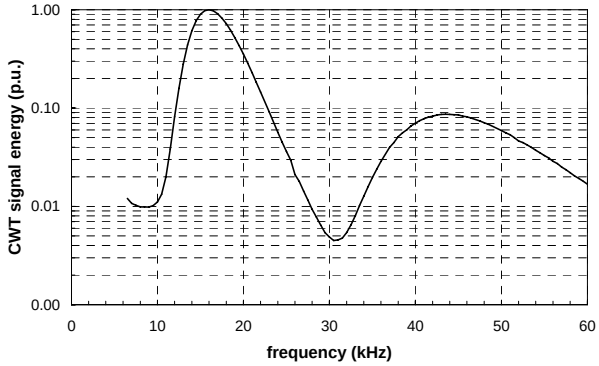

Figure 4 Results of the CWT analysis of the volateg transient at bus 4, due to a zero-impedance three-phase fault at bus 5. The values are in per unit with respect to the maximum ($3.66 \cdot 10^{12}$ V^2s).

Table 2 Frequency values theoretically associated to the paths covered by the traveling waves originated by a balanced fault at bus 5, and values identified by the CWT analysis.

Path	length	theoretical frequency (traveling wave at light speed) (kHz)	CWT identified frequency (kHz)
L1+L2	4x5km	15	16.0
L1+L5	2x3km	50	43.5

Figure 5 and Table 3 show the results for the case of a balanced fault at bus 2, which is the termination of a lateral. In this case three paths are of interest: a) L1+L2+L4, with opposite sign reflections at the fault location (bus 2) and at the main feeder sending end (bus 4), b) L1+L2+L3 and c) L1+L5, with reflections at the line terminations. The CWT analysis, performed by using the Morlet mother wavelet, is able to detect only the frequencies associated with two paths, namely the first and the third ones, while the frequency peak associated with the second path appears to be hidden by the first peak due to the large filter amplitude related to the adopted mother wavelet.

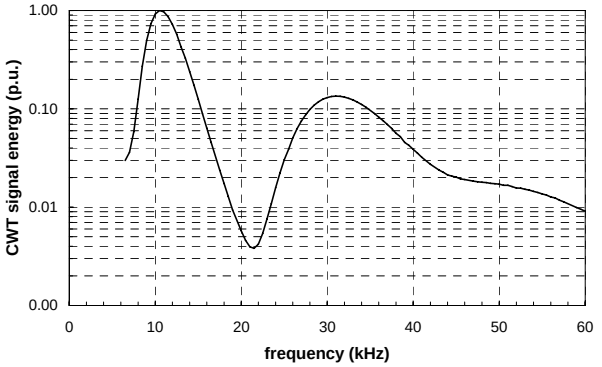

Figure 5 Results of the CWT analysis of the voltage transient at bus 4, due to a zero-impedance three-phase fault at bus 2. The values are in per unit with respect to the maxi-mum ($1.71 \cdot 10^{12}$ V^2s).

Table 3 Frequency values theoretically associated to the paths covered by the traveling waves originated by a balanced fault at bus 2, and values identified by the CWT analysis.

Path	length (km)	theoretical frequency (traveling wave at light speed) (kHz)	CWT identified frequency (kHz)
L1+L2+L4	4x7	10.7	10.5
L1+L2+L3	2x10	15.0	-
L1+L5	2x6	25.0	31.0

The influence of the presence of distributed generation has been also investigated. We have repeated the analysis for balanced faults at bus 1 and bus 5 in presence of a generator connected at bus 2 through a transformer. The CWT identified frequency values are very similar to those of Table 1 and Table 2, showing that the presence of the generator does not modify significantly the reflection coefficients at the line termination.

2.2 Nonsymmetrical faults

For the case of nonsymmetrical faults, the different propagation velocities of the various modes of the traveling waves must be taken into account [6]. Therefore, the CWT based analysis has been carried out separately

on the various modes present in the voltage transient recorded at the observation point.

Equations (4) and (5), written in the frequency domain, summarize the modal transformation, as a way to make diagonal the matrixes given by the products [*Z'*][*Y'*] and [*Y'*][*Z'*]. These matrixes are not equal, but have the same eigenvalues that, squared, form the diagonal matrix $[\gamma]^2$.

$$\left[\frac{d^2V^f}{dx^2}\right] = [Z'][Y']\left[V^f\right]$$
$$\left[\frac{d^2I^f}{dx^2}\right] = [Y'][Z']\left[I^f\right] \quad (4)$$

$$\left[\frac{d^2V^m}{dx^2}\right] = [\gamma]^2\left[V^m\right]$$
$$\left[\frac{d^2I^m}{dx^2}\right] = [\gamma]^2\left[I^m\right] \quad (5)$$

Coefficients γ_i are the propagation constant of mode *i*. They are complex numbers $\gamma_i = \alpha_i + j\beta_i$ where α_i is the attenuation constant and β_i is the phase constant of mode *i*. The phase velocity of mode *i* is given by

$$v_i = \frac{\omega}{\beta_i} \quad (6)$$

The columns of transformation matrixes $[T_e]$ and $[T_i]$, that make diagonal matrix [*Z'*][*Y'*] and matrix [*Y'*][*Z'*], respectively, are given by corresponding linear independent eigenvectors. For the case of balanced lines or lines, transformation matrixes $[T_e]$ are $[T_i]$ identical and can be composed by real numbers, i.e. they correspond to the Clarke's (0,α,β) transformation matrix:

$$[T_i] = [T_e] = \frac{1}{\sqrt{3}}\begin{bmatrix} 1 & \sqrt{2} & 0 \\ 1 & -\frac{1}{\sqrt{2}} & \frac{\sqrt{3}}{\sqrt{2}} \\ 1 & -\frac{1}{\sqrt{2}} & -\frac{\sqrt{3}}{\sqrt{2}} \end{bmatrix} \quad (7)$$

Considering the line configuration shown in the Appendix, as a first approximation, the Clark transformation is applied to the voltage transients at the observation point (bus 4) of the distribution network of Figure 1, for different types of unbalanced faults at various locations, also with nonzero fault impedances.

Figure 6 illustrates the results of the CWT analysis of the voltage transients due to a phase-to-ground fault at bus 1, both for the case of a grounded and ungrounded neutral.

Also in this case, the considered paths are those illustrated in Figure 1. The phase velocity of mode 0 is however significantly lower than speed of light (as shown in Table 8 of the Appendix). This velocity is used to evaluate the theoretical frequency values, which, in Table 4, are compared with those identified by the CWT analysis.

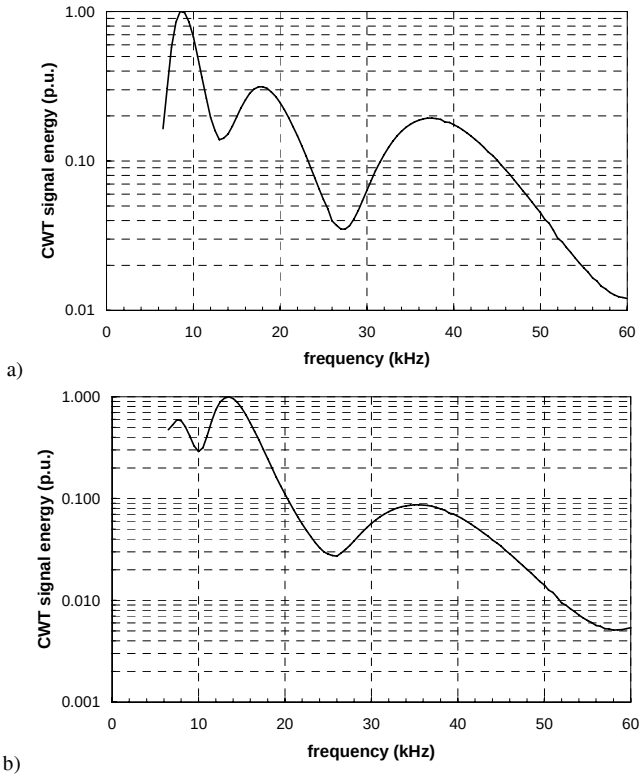

Figure 6 Results of the CWT analysis of mode 0 of the voltage transient at bus 4, due to a phase-to ground fault at bus 1: a) grounded neutral network, b) ungrounded neutral. The values are in per unit with respect to the maximum ($1.37 \cdot 10^9$ V^2s and $1.74 \cdot 10^{11}$ V^2s for the case of grounded and ungrounded neutral, respectively).

Table 4 Frequency values theoretically associated to the paths covered by the traveling waves originated by a phase-to-ground fault at bus 1, and values identified by the CWT analysis.

path	length (km)	theoretical frequency (mode 0) (kHz)	CWT identified frequency (kHz)
neutral grounded			
L1+L2+L3	4x10	6.1	8.5
L1+L2+L4	2x7	17.3	18.0
L1+L5	2x3	40.4	37.0
neutral ungrounded			
L1+L2+L3	4x10	6.1	7.5
L1+L2+L4	2x7	17.3	13.5
L1+L5	2x3	40.4	36.0

Table 5 shows the results for the similar case of a phase-to-ground fault at bus 5.

Table 5 Frequency values theoretically associated to the paths covered by the traveling waves originated by a phase-to-ground fault at bus 5, and values identified by the CWT procedure.

path	length (km)	theoretical frequency (mode 0) (kHz)	CWT identified frequency (kHz)
neutral grounded			
L1+L2	4x5	12.1	15.0
L1+L5	2x3	40.4	38.0
neutral ungrounded			
L1+L2	4x5	12.1	12.0
L1+L5	2x3	40.4	33.0

We have repeated the simulations and the analysis also by taking into account a fault resistance equal to 10 Ω, and quite the same results as those shown in Table 4 and Table 5 have been obtained. Also the presence of unbalanced loads does not appear to have evident impacts on the results.

Table 6 shows the results for the case of a phase-to phase fault, and Table 7 shows the results obtained for a two phase-to-ground fault. For both cases, two fault locations are examined: bus 1 and bus 5. The neutral is considered ungrounded.

Table 6 Frequency values theoretically associated to the paths covered by the traveling waves originated by a phase-to-phase fault at bus 1 and at bus 5 (neutral ungrounded), and values identified by the CWT procedure.

path	length (km)	theoretical frequency (modes α and β) (kHz)	CWT identified frequency (kHz)
Fault location at bus 1			
L1+L2+L3	4x10	7.4	9.5
L1+L2+L4	2x7	21.0	20.5
L1+L5	2x3	49.0	50.5
Fault location at bus 5			
L1+L2	4x5	14.7	16.0
L1+L5	2x3	49.0	43.5

Table 7 Frequency values associated to the paths covered by the traveling waves originated by a two phases-to-ground fault at bus 1 and bus 5 (neutral ungrounded), and values identified by the CWT procedure.

path	length (km)	theoretical frequency (kHz)		CWT identified frequency (kHz)	
		mode 0	modes α-β	mode 0	modes α-β
Fault location at bus 1					
L1+L2+L3	4x10	6.1	7.4	4.5	9.5
L1+L2+L4	2x7	17.3	21.0	14.5	20.5
L1+L5	2x3	40.4	49.0	37.0	49 - 50
Fault location at bus 5					
L1+L2	4x5	12.1	14.7	10.5	16.0
L1+L5	2x3	40.4	49.0	33.0	43.5

Although some of the results show some limits of the adoption of the Morlet wavelet, namely those relevant to fault at the laterals of the network in Figure 1 (e.g. balanced fault at bus 2), overall we have achieved a reasonably good match between the theoretical values and the CWT identified frequencies. Such a match encourages the development of a fault location system exploiting this information. To this subject we devote the next section.

3 ACQUISITION SYSTEM WITH DISTRIBUTED ARCHITECTURE

The described CWT based algorithm is conceived to be combined with a distributed measurement system. Each unit, located at some suitable busses of the distribution network, is equipped with a GPS synchronization device and is able to acquire both the starting instant of the transient and the relevant waveform.

A measurement unit of the fault-location distributed system is schematically represented in Figure 7, which represents an improvement of the one presented in [7].

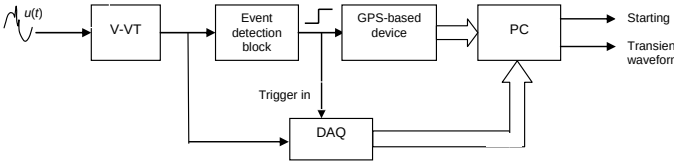

Figure 7 Schematic block diagram of the measurement system

Each line voltage is conditioned by means of a voltage-to-voltage transducer (V-VT) whose output is sent both to an Event Detection Block (EDB) and to an analog-to-digital conversion board (DAQ). The EDB is specifically designed to detect the presence of transients superimposed to the supply voltage waveform and provides a logic signal that, at the occurrence of a transient, acts as a pretrigger for the DAQ for the data acquisition and as a trigger for the GPS-based device in order to record the starting time of the transient. The DAQ output is off-line analyzed through the above described algorithm.

A prototype of the unit has also been realized, with the following characteristics. A voltage-to-voltage capacitive-divider VD-305A has been used, with insulation voltage 300kV peak, nominal ratio 10000V / 1V, bandwidth 30Hz ÷ 4MHz (-3dB), rising time 100ns, accuracy ±1%. Its output signal feeds the event detection block, which has been implemented by means of an analog circuit described in [7]. Its output is a TTL dual-logic signal, in conformity with the requirements of the GPS-based device (GPS168PCI [8]). This device captures the time instant of a falling edge of its input, with a nominal accuracy of ±250ns. Moreover, it provides TTL pulses, with 1s period and a nominal accuracy of ±250ns, used to synchronize all the functions performed by the measurement system. The comparison of the time instants of the received voltage transients at different distributed measurement unit improves the accuracy of the location of the faulted section, provided by the CWT analysis.

A 12-bit acquisition device is used, with a maximum sampling frequency of 100MSa/s, a nominal accuracy is ±1% and a storage capability of 64kb of data, allowing an acquisition window of 10ms with a sampling rate of 3.2MSa/s.

The instrument is also equipped with a GSM/GPRS modem for data transmission/reception. Such a system has been designed to operate according to a master-slave architecture.

3.1 Analysis of the measurement uncertainty

The uncertainty sources, whose effects propagate through the measurement algorithms and determine the combined standard uncertainty, are mainly located in the measurement hardware. In this Section, a preliminary analysis is performed, aimed at evaluating the uncertainty affecting the estimate of fault location start-

ing from the samples acquired by the described instrument.

The ISO "Guide to the expression of uncertainty in measurement" [9] prescribes an analytical procedure for evaluating the uncertainty affecting indirect measurements starting from the uncertainties affecting the input quantities. However in our case, as in many other many practical situations, the uncertainty evaluation provided by means of such an analytical procedure is inapplicable. The uncertainty evaluation is therefore carried out by means of a numerical technique, based on the simulation of a statistical meaningful number of measurements in order to estimate the relevant probability density function (pdf). Specifically, the first step of the procedure is the characterization of the metrological performance of each device of the measurement system, in order to obtain the pdf of uncertainty sources. This evaluation can be performed by preliminary experimental tests on every device or from the nominal accuracy specifications provided by the manufacturers. Once these distributions are known, populations of random variables having the desired statistical parameters associated to the uncertainty contributions are generated and a large number of simulations, by using the measurement algorithm, are performed, starting from input data corrupted by different values of the uncertainty contributions randomly extracted from the above mentioned populations. At the end of the procedure, a population of measurements is obtained and the relevant pdf is estimated.

This procedure has been applied to our case, starting from the nominal accuracy specifications provided by the manufacturers. In particular, as already mentioned, two accuracy specifications are provided: ±1% accuracy level for the transducer nominal ratio and ±1% for the DAQ. In the lack of further information, independent uniformly-distributed random variables have been used to represent the effects of these uncertainties sources.

The tests performed on different networks configuration have shown uncertainty levels lower than 200Hz on the estimate of the frequency associated to the paths covered by the travelling waves. This value provides an indication of the uncertainty of the estimated fault location, as a function of the length of the path and the propagation velocity.

4 CONCLUSIONS

The paper has illustrated a method based on the continuous-wavelet transform for the analysis of voltage transients due to a short circuit. The analysis carried out allows inferring that a correlation exists between some characteristic frequencies of the transformed signal and specific paths in the network, covered by the traveling waves originated by the fault.

The results show that acceptable fault location is provided by the proposed procedure, for the considered network configurations and type of faults. Additional research efforts will be devoted to take into account more complex configurations of the distribution network (e.g. having both overhead lines and cables) and to the selection of improved mother wavelets.

Further, the authors feel that the obtained results may constitute the basis for the development of a fault location system, having distributed architecture, which exploits the achieved information.

REFERENCES

[1] O. Chaari, M. Meunier, F. Brouaye, "Wavelets: a new tool for the resonant grounded power distribution systems relaying", IEEE Trans. on Power Delivery, vol. 11-3, pp. 1301-1308, July 1996.

[2] F.H. Magnago, A. Abur, "Fault location using wavelets", IEEE Trans. on Power Delivery, vol. 13-4 , Oct. 1998, pp. 1475-480.

[3] S. Hanninen, M. Lehtonen, T. Hakola, R. Rantanen, "Comparison of Wavelet and Differential equation algorithms in earth fault distance computation", Proc. PSCC'99, Trondheim, Norway, 1999.

[4] H. Nouri, Chun Wang; T. Davies, "An accurate fault location technique for distribution lines with tapped loads using wavelet transform", Proc. 2001 IEEE Power Tech, Porto , vol. 3 , 10-13 Sept. 2001.

[5] L. Angrisani, P. Daponte, M. D'Apuzzo, "Wavelet network-based detection and classification of transients", IEEE Trans. on Instrumentation and Measurement, vol. 50-5, Oct. 2001, pp. 1425 – 1435.

[6] H. W. Dommel, "Digital computer solution of Electromagnetic Transients in single and multi-phase networks", IEEE Transactions on Power Apparatus and Systems, Vol. PAS-88, pp. 388-399, April 1969.

[7] L. Peretto, P. Rinaldi, R. Sasdelli, R. Tinarelli, "A System for the Measurement of the Starting Instant of Impulsive Transients", Proc. of the 21st IEEE IMTC/04, Como (Italy), 18-20 May 2004, vol 2, pp. 1394-1398.

[8] Meinberg Funkuhren, "GPS168PCI: Technical Information – Operating Instructions", Bad Pyrmont (Germany), June 2002.

[9] ISO "Guide to the expression of uncertainty in measurement", International Standardization Organization, Geneva (Switzerland), 1995.

[10] J. Marti, "Accurate Modelling of Frequency Dependent Transmission Lines in Electromagnetic Transient Simulations", IEEE Trans. on Power Apparatus and Systems, vol. PAS-101, pp. 147-157, 1982.

APPENDIX

In this paper, the CWT analysis has been carried out by means of simulation results obtained, for the power distribution network configuration illustrated in Figure 1, using an electromagnetic transient program, namely the EMTP-RV package.

The distribution network is composed by a 10km long main feeder (lines L1, L2 and L3) and by two laterals of 2km length (L4) and 1km length (L5). The

power distribution network is supplied by a 150/20 kV substation.

The characteristics and conductor's geometry of the overhead lines is shown in Figure 8. The ground resistivity is assumed equal to 100Ωm.

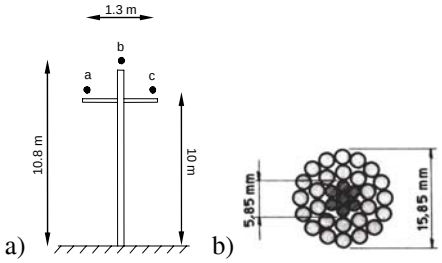

Figure 8 Configuration of the overhead line and cross-section of the conductors.

The lines are represented by a "constant parameter line model" (CP-line model) [6] and the values of the line modal parameters are reported in Table 8. It is worth mentioning that the adoption of a frequency dependent line model (e.g. the FD-line model [10]) results in voltage transients close to those obtained with the CP-line model. This is due on the one hand to the typically limited length of distribution lines and, on the other hand, to the typical frequency content of the fault transients, which does not exceed a few tens of kHz.

Two types of power transformers are present: (i) a 20 MVA 150/20 kV transformer at the substation and (ii) 3MVA 20/0.4 kV distribution transformers at the load busses. Figure 9 illustrates the load blocks connected at busses 1, 2 and 3 of Figure 1. Each load is connected at the low voltage side of the distribution transformer and is represented by three impedances. A Π of capacitance is also included in parallel at each transformer model order to simulate, in a first approximation, its response to transients at a frequency range around 100 kHz.

Table 8 Value of the modal parameters of the overhead line of Figure 8 above a ground with resistivity equal to 100Ωm.

mode	r (Ω/km)	l (mH/km)	c (μF/km)	z_c (Ω)	phase velocity (km/s)
0	3.600	4.151	$4.079 \cdot 10^{-03}$	1011.90	$2.426 \cdot 10^{+05}$
α	0.353	1.030	$1.121 \cdot 10^{-02}$	303.24	$2.941 \cdot 10^{+05}$
β	0.353	1.030	$1.121 \cdot 10^{-02}$	303.24	$2.941 \cdot 10^{+05}$

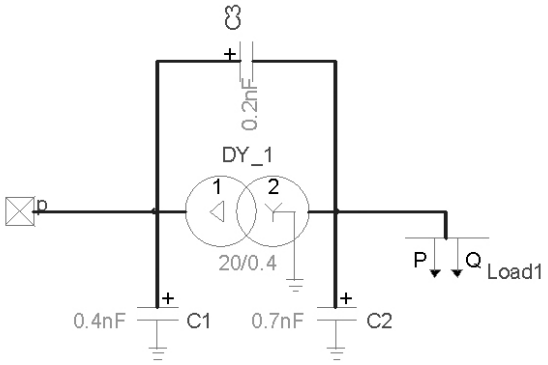

Figure 9 Configuration of the load blocks